Journal of Alloys and Compounds 819 (2020) 152979

Contents lists available at ScienceDirect

Journal of Alloys and Compounds

journal homepage: http://www.elsevier.com/locate/jalcom

Effect of the fictive temperature on the modulus, hardness, yield strength, dynamic mechanical and creep response of $Zr_{44}Ti_{11}Cu_{10}Ni_{10}Be_{25}$ metallic glasses

Amit Datye [a, *], Jittisa Ketkaew [a], Jan Schroers [a], Udo D. Schwarz [a, b, **]

[a] Department of Mechanical Engineering and Materials Science, Yale University, New Haven, CT, 06511, USA
[b] Department of Chemical and Environmental Engineering, Yale University, New Haven, CT, 06511, USA

ARTICLE INFO

Article history:
Received 27 July 2019
Received in revised form
12 October 2019
Accepted 10 November 2019
Available online 11 November 2019

Keywords:
Bulk metallic glass
Fictive temperature
Nanoindentation
Dynamic mechanical analysis
Creep

ABSTRACT

Characterizing the dependence of the mechanical properties and structure of metallic glasses on processing parameters and thermal history is of significant importance to understand the nature of glass. One way of defining a specific structural state of a glass is by means of its fictive temperature T_f at which the supercooled liquid falls out of a metastable equilibrium and forms a glass. Since the metastable equilibrium state before quenching is assumed to be well defined, T_f is ultimately thought of as a quantity that describes a specific, reproducibly obtainable structural state. In this research, the effect of systematic variations of an alloy's structural state, achieved through purposefully setting its T_f, on a range of mechanical properties like modulus, hardness, yield strength, and creep response is studied. Towards this end, amorphous $Zr_{44}Ti_{11}Cu_{10}Ni_{10}Be_{25}$ samples with different T_f's were produced and subsequently examined using nanoindentation, dynamic mechanical thermal analysis, and density measurements. It is observed that the lower fictive temperatures directly result in a higher the packing efficiency, i.e., a lower available ('free') volume in the glass. The resulting denser atomic packing manifests in increased values for hardness, modulus, and yield strength. These effects were found to be substantial despite the fact that all samples featured the exact same chemical composition and phase.

1. Introduction

Metallic glasses, which were first discovered in 1960 [1], enable technological applications that are distinct from what can be achieved with conventional materials due to the unusual mechanical, physical, and chemical properties they exhibit [2–5]. In addition, they possess promising mechanical properties, such as superior strength and hardness and a high elastic strain limit [2]. Originally only available as rapidly quenched thin films and ribbons [6,7], developments for this class of materials have significantly accelerated since alloy systems became available that allow the prolonged processing of amounts large enough to manufacture items usable in daily life [6,7]. With these so-called *bulk metallic glasses* (BMGs) [8,9], applications ranging from eyeglass frames, surgical tools, and biomedical implants to golf clubs have been realized [4,5].

In conventional polycrystalline metals and alloys, the atomic-level structure is generally well defined, consisting mainly of ordered dense packing with less ordered regions featuring defects such as dislocations and grain boundaries. Since glass is an amorphous solid made by quenching a melt, it lacks long-range positional order [10,11]. Most glasses, both traditional (i.e., silica and other oxide-based glasses) and metallic, have nevertheless been found to possess short-to-medium range order [12]. Oxide glasses are essentially ideally brittle with no appreciable room-temperature plasticity due to the high energy barriers related to permanent deformations, which makes them extremely flaw-sensitive with fracture toughness determined by the size and distribution of flaws [13,14]. In contrast, while metallic glasses are disordered like traditional glasses, they also feature mostly metallic bonds [3], which results in unique mechanical properties by enabling a range of deformation mechanisms [4,5]. However, there is insufficient understanding of the structure–processing relationships in BMGs, which is needed to predict, design, and optimize their mechanical behavior.

To advance our respective understanding, it is important to note that the structure of BMGs, and with it their properties, are not only

* Corresponding author.
** Corresponding author. Department of Mechanical Engineering and Materials Science, Yale University, New Haven, CT, 06511, USA.
E-mail addresses: amit.datye@yale.edu (A. Datye), udo.schwarz@yale.edu (U.D. Schwarz).

https://doi.org/10.1016/j.jallcom.2019.152979
0925-8388/

defined by their chemical composition, but also by their degree of relaxation, which is sensitive to their processing conditions. Different structural states are often described in terms of their so-called *fictive temperature* T_f [8,15–17], which is the temperature where the structure of a supercooled liquid first deviates from its metastable equilibrium state; since these equilibrium states are thought to be well defined, each T_f denotes a specific structural state with a consistent set of properties. For example, if, upon cooling, the supercooled liquid falls out of metastable equilibrium at a relatively high temperature, it 'freezes in' the considerable disorder this temperature induced in the liquid, which is expected to lead to more free volume and thus to a lower density compared to specimen prepared at lower T_f. After cooling to room temperature, the resulting BMG's glassy state is then characterized by an unfavorably high value for its cohesive energy (typically referred to in terms of its 'potential energy'), which is reflected in a high fictive temperature. The opposite is the case for slow cooling, which enables the alloy to relax further before departing from a metastable equilibrium state, thereby assuming states of lower potential energy.

In earlier work, we have already shown that describing structural states by their fictive temperatures represents an insightful method of evaluating variations in a sample's fracture toughness [15]. Here we demonstrate with the example of a glassy $Zr_{44}Ti_{11}Cu_{10}Ni_{10}Be_{25}$ alloy that this concept goes beyond fracture toughness, as samples of identical chemical composition, but exposed to different thermal processing histories, were found to exhibit distinct sets of a wide range of mechanical properties. In this context, it is important to note that due to its importance, the influence of thermal processing on the structure of BMGs and the effect of annealing on the structure and properties like density [18,19], modulus [19–24], and plasticity [25–27] has been previously been studied. Thereby, the observed changes in structure and properties have been attributed to structural relaxation [28], an increase in short-range ordering [18,20], free volume reduction [21,25,29,30], a decrease in STZ volume [31], and phase separation [32]. The work presented in this paper distinguishes itself in two key points: First, we correlate the material's structural state to a specific fictive temperature rather than to annealing protocols that are mostly heuristic in nature, the variations in properties can be tracked *as a function of a well-defined structural evolution* the BMG is undergoing.

To validate the usefulness of this approach, we show that lower fictive temperatures indeed lead to higher densities, corroborating both this parameter's value as a qualifier for the material's structural state as well as the effectiveness of our sample preparation methodology. Second, previous research has focused on measuring selected properties on each sample. This allows to formulate expectations of how different properties measured on different samples and in different studies may correlate, but does not verify their exact interrelations. In contrast, we *systematically track how higher densities translate into increased values for modulus, hardness, yield strength, and creep response*. Generalizing from the underlying principles can therefore help to establish an understanding of processing-property relationship of BMGs that may serve as a guideline when attempting to customize materials properties to best fit specific desired functions.

2. Materials and methods

2.1. Preparation of samples with different fictive temperatures

For the present studies, we used a research grade $Zr_{44}Ti_{11}Cu_{10}Ni_{10}Be_{25}$ BMG (Zr-BMG) plate 120 mm × 100 mm × 5 mm in size supplied by Materion (Mayfield Heights, Ohio). The manufacturer

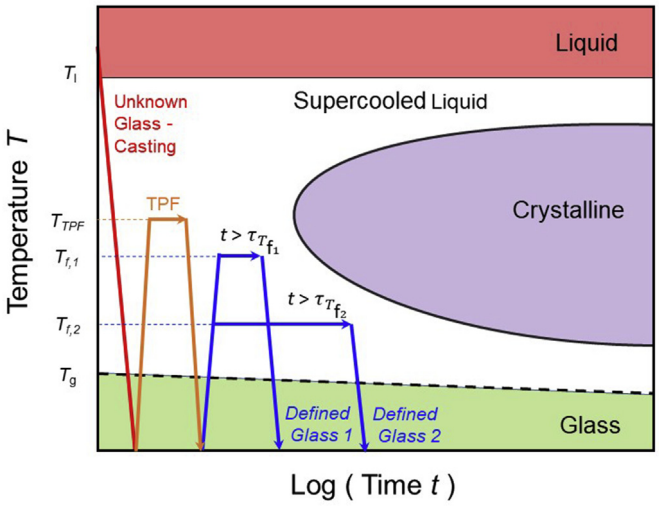

Fig. 1. Graph representing the thermal treatment of samples used in the present studies. The red curve reflects the treatment the raw alloy experienced during casting at the manufacturer's facility (red curve). Once in house, the samples were pressed into shape by thermoplastic forming (orange curve), followed by the annealing process that induces structural states defined by T_f. Thereby, the respective blue curves visualize the procedure for two different values, $T_{f,1}$ and $T_{f,2}$, which both have different relaxation times τ. (For interpretation of the references to colour in this figure legend, the reader is referred to the Web version of this article.)

specified the alloy's glass transition temperature T_g, crystallization temperature T_x, and melting temperature T_m as $T_g = 352\,^{\circ}C$, $T_x = 466\,^{\circ}C$, and $T_m = 644\,^{\circ}C$ [33]; in a separate study, the liquidus temperature T_l, Young's modulus E, and the shear modulus G of the material were found to be $T_l \approx 726\,^{\circ}C$, $E = 95.2$ GPa, and $G = 35.1$ GPa, respectively [34]. The amorphous state of the as-cast plate as well as all samples after setting specific fictive temperatures was confirmed by differential scanning calorimetry and X-ray diffraction (Rigaku Smartlab XRD). The preparation procedures for Zr-BMG samples with different fictive temperatures are illustrated in Fig. 1. The underlying principle is that upon annealing a sample with unspecified thermal history at a fixed temperature T, the BMG transitions through a large number of structural states until, after having been heated for a time period longer than its 'relaxation time' defined by the Vogel-Fulcher-Tammann (VFT) relation for relaxation times [33,35,36].

$$\tau(T) = \tau_0 \exp\left(\frac{D^* T_0}{T - T_0}\right), \tag{1}$$

it ultimately approaches a metastable equilibrium state. Thereby, $T_0 = 344.64\,^{\circ}C$ represents the temperature at which $\tau \to \infty$, τ_0 reflects a minimal relaxation time established at 'very high' temperatures (i.e., $T \to \infty$; τ_0 is estimated to be ~2.5×10^{-13} s for Zr-BMG systems [37,38]), and $D^* = 28.1338$ is a constant referred to as the 'fragility parameter' [38,39]. An unknown glass obtained from casting would find a new, well-defined metastable equilibrium state by annealing at $T_{f,1}$ with a relaxation time t_{relax} exceeding $\tau_{T_{f,1}}$; accordingly, annealing with $T_{f,2} < T_{f,1}$ instead will lead to a different, but also well-defined state after having heated for the appropriate time $\tau_{T_{f,2}} > \tau_{T_{f,1}}$ obtained from the VFT law. When followed by rapid quenching, these states are defined (meaning that they are thought to feature consistent macroscopic observables such as Young's modulus, hardness, density, etc.) as long as their respective annealing temperatures T_f, referred to as their fictive temperatures [8,15–17,33], are reported. Due to their exponential dependence, t_{relax} varies substantially from, e.g., $t_{relax} \approx 0.7$ s with $T_f = 410\,^{\circ}C$

over $t_{relax} = 32$ s for $T_f = 370\,^{\circ}C$ to t_{relax} just above 6 h for $T_f = 320\,^{\circ}C$ [37]. To avoid any structural transformation induced by the onset of crystallization, $\tau_{T_f,1}$ should at the same time be chosen to be much shorter than the time needed for crystallization, with the onset of crystallization for Zr-BMG determined by differential scanning calorimetry (PerkinElmer Diamond DSC) to ≈12 min for $T_f = 410\,^{\circ}C$ and ≈100 min for $T_f = 370\,^{\circ}C$; by means of extrapolation, it had previously been estimated to >10 years for $T_f = 320\,^{\circ}C$ [37,40].

Fig. 1 illustrates the thermal histories of the samples used in the present studies while distinguishing the preparation routes for two different fictive temperatures T_f. After rapid quenching (red curve), samples were shaped into testing geometry through thermoplastic forming [34,41–43] by heating at 420 °C for 2 min under a compressive force of 1 kN followed by a subsequent water quench, which is also expected to eliminate most of the casting defects (orange curve). Annealing (blue curves) was then carried out by heating the samples inside a furnace with a temperature ramp of 20 K/min; after the desired temperature was reached, the samples were kept at this temperature for the at least 1.5 times the time period t_{relax} given by the VFT equation always followed by rapid quenching in water. Finally, standard metallurgical sample preparation techniques such as cutting and polishing were employed as needed to prepare the samples for nanoindentation (4 mm × 3 mm × 2 mm cubes) and dynamic mechanical analysis (~30 mm × 3 mm × 2 mm).

2.2. Density measurements

Samples used for density measurements, which were at least 1 g in weight, were first cleaned ultrasonically in acetone and then carefully weighed using a Mettler Toledo XS205 DU balance with a resolution of 0.01 mg. An average of four sample were made at each fictive temperature to account for possible fluctuations. To determine the skeletal density [44] of the glasses, at least ten consecutive measurements were then performed on each sample using a Micromeritics AccuPyc™ 1330 pycnometer with 1 cm^3 cell and with helium as the gas for each fictive temperature characterized. Following these procedures, the standard deviation for the volume measurements by helium pycnometry was 0.001 cm^3 while the weight measurements featured a standard deviation of 0.02 mg.

2.3. Mechanical properties measurement

2.3.1. Nanoindentation using Berkovich and spherical indenters

Nanoindentation testing in continuous stiffness measurement (CSM) [45] mode with a peak load of 50 mN was carried out using a Nanoindenter XP system (Nanomechanics Inc., Oak Ridge, TN) featuring a resolution of 0.2 nN and a Berkovich tip calibrated on standard fused silica samples for contact area with respect to the indentation depth [46]. An average of 16 indents was taken for both modulus and hardness measurements. To relate the stiffness $S = dP/dh$ to the *reduced modulus* or *Hertz modulus* E^* of the material, we apply an equation developed in the 1970ies by Bulychev, Alekhin, Ternovskii, and co-workers [47–50].

$$S = \frac{dP}{dh} = 2E^* \frac{\sqrt{A}}{\sqrt{\pi}}, \tag{2}$$

where P is the load on sample and h the displacement of the indenter into the surface ('indentation depth'), and $E^* = ((1 - \nu_m^2)/E_m + ((1 - \nu_i^2)/E_i)^{-1}$ is obtained from Young's modulus and Poisson's ratio of the sample (E_m, ν_m) and the indenter material ($E_i = 1141$ GPa, $\nu_i = 0.07$ for diamond), respectively. Oliver and Pharr in 1992 [46] demonstrated that Eq. (2), originally developed for conical and cylindrical indenters, is also valid for axisymmetric indenters with an infinitely smooth profile and can be used to determine the elastic properties of a material. While the loading segment in a nanoindentation experiment for a majority of materials is elastic-plastic, the unloading stage is purely elastic. Since BMGs can be assumed to be elastically isotropic materials, the *effective modulus* for the material during indentation is given by Refs. [51–53].

$$E_{Effective} = E_m \Big/ \left(1 - \nu_m^2\right), \tag{3}$$

As the amount of pile up or sink-in during indentation is unknown, the Oliver-Pharr hardness H, which is calculated as load over the contact area assuming sink-in behavior, is reported. Tabor [54] observed that the ratio of hardness H to yield strength (flow stress) σ_y is approximately equal to 3; this relationship prevails when the strain e is approximately 0.08, which is the average plastic strain for a Vickers indenter regardless of the initial state of strain hardening [55–57]. Referred to as *Tabor's equation* in the following, $H/\sigma_y \approx 3$ has been shown to be theoretically and experimentally valid for non-strain hardening materials like BMGs [57,58].

Nanoindentation creep testing was carried out using a spherical 10 μm diameter diamond tip up to a peak load of 100 mN (to ensure an elastic-plastic response) at a loading and unloading rate of 200 mN/min using an Anton Paar NHT-3 instrument on the same Zr-BMG samples with different T_f used in the Berkovich nanoindentation experiments. The hold time at maximum load was 180 s, and at least 16 indents were completed on each sample with the average being reported. A generalized Kelvin-Voight model using one element was then applied to analyze the data. Within this model, the material creep response during spherical indentation is described by a creep function [59–61].

$$J(t) = C_o - C_1 \exp\left(-t/\tau_1\right) \tag{4}$$

where $J(t)$ is the strain response to the unit step of stress as a function of time t and is referred to as 'creep compliance', while τ_1 is the retardation time and C_0 and C_1 are constants. The indentation depth h, which combines both the elastic ("h_e") and plastic ("h_p") contributions to the total displacement into the surface, then follows as [59].

$$h^{1.5}(t) = B_o - B_1 \exp\left(-t/\tau_1\right) \tag{5}$$

where B_0 and B_1 are constant terms. Fitting Eq. (5) for indentation depth h and time on sample t data from the start of hold at peak load to the end of hold at peak load yields B_0, B_1, and τ_1 [59,60]. The relative change in the indentation depth during the hold segment C_{IT} (i.e., $C_{IT} = (h_2 - h_1) \times 100/h_1$, where h_1 and h_2 are the indentation depths at hold times $t_1 = 0$ s and $t_2 = 180$ s respectively), and the Hertz modulus E^* is then calculated based on the load displacement curve and the radius of the indenter using a Poisson's ratio of 0.35 for the Zr-BMG [45,46,53].

2.3.2. Dynamic mechanical analysis

The variation of the storage modulus G' (measure of the elastic response), the loss modulus G'' (measure of the viscous response) and the tan δ (measure of the energy dissipation) of the material in torsion with temperature was studied using a TA Instruments Ares G2 dynamic mechanical analyzer operated in the isochronal (i.e., scanning temperature at fixed frequency) mode. The samples were examined with 0.01% strain at 1.5 Hz frequency from room temperature T_r to −150 °C and from T_r to 400 °C at 5 °C per min ramp

rates while keeping them in 0.1 N (≈ 10 g) auto-tension. During the analysis, the complex modulus $G = G' + iG''$ is first obtained from experimental data, from which storage modulus G', loss modulus G'', and loss factor $\tan\delta = G''/G'$ are determined. Dynamic mechanical analysis (DMA) of samples with different T_f also allows us to study the influence of sample thermal history (i.e., structure) on the relaxation dynamics (α and β relaxations) in the bulk metallic glass. Thereby, the α relaxation is linked to effects occurring at the glass transition temperature, while β relaxation is thought to be related to the degree of local structural heterogeneity and manifests below the glass transition temperature.

3. Results and discussion

3.1. Validating the fictive temperature as a qualifier for the BMG's structural state

3.1.1. Differential scanning calorimetry and XRD

The required fast cooling for the formation of BMGs results in a significant amount of imperfections like shear transformation zones [62], stress inhomogeneities, and free volumes [63,64] entrapped in the matrix, the degree of which depends on how much time the glass is given to relax. Out of these imperfections, the free volume has been found to be a particularly important structural feature in amorphous alloys, significantly affecting the mechanical, physical, and chemical properties [38,65,66]. More specifically, Evenson et al. [66] Slipenyuk et al. [67] and Haruyama et al. [68] noted correlations between enthalpy changes and free volume reduction during structural relaxation. In the differential scanning calorimetry (DSC) measurements presented in Fig. 2a, we observe that Zr-BMG processed with higher fictive temperatures ($T_f = 410\,^\circ$C and $370\,^\circ$C, respectively) shows significantly less exothermic heat flux from structural relaxations than BMG processed with lower fictive temperature ($T_f = 320\,^\circ$C).

The enthalpy recovered from glasses with low fictive temperature needs therefore to be greater than that of glasses with higher fictive temperature, indicating that glasses with higher T_f must contain comparatively more free volume and vice versa, in agreement with the expectations discussed in the introduction. Ultimately, these conclusions simply reflect the fact that the lower thermal energy available at lower fictive temperatures results in the annihilation of excess free volume present in the glass as long as sufficient time to structurally relax is provided [67].

XRD measurements on samples with different fictive temperatures shown in Fig. 2b do not show any obvious peaks indicating that the samples are fully amorphous after annealing at different fictive temperatures.

3.1.2. Density measurements

Density measurements for samples prepared at four different fictive temperatures T_f showed a clear trend that samples processed at lower T_f feature higher densities. The measured densities were 6.0736 ± 0.002 gm/cm^3, 6.0651 ± 0.003 gm/cm^3, 6.0584 ± 0.002 gm/cm^3, and 6.0505 ± 0.002 gm/cm^3 for samples with $T_f = 320\,^\circ$C, $350\,^\circ$C, $370\,^\circ$C and $T_f = 410\,^\circ$C, respectively, which results in a basically linear decrease of the specimen's density with increasing T_f according to $2.57 \times 10^{-4} \times T_f$ - 6.155 with an R^2 value of 0.997. These measurements corroborate the conclusions and anticipations of the previous section that the thermal annealing process associated with setting a specific value of T_f shrinks excess free volume to the effect that lower T_f induce higher densities. It has also been shown in our previous research that an increase in fictive temperature results in a broader structure function S(Q), and a lower amplitude of the first peak of the pair distribution; which indicates a higher degree of disordering as fictive temperature increases [15]. Having this expectation in mind, perhaps most remarkable aspect of the data is therefore not the general trend, but its substantial manifestation (≈ 0.38% variation between the densest and least dense sample despite identical chemical composition), which validates the effectiveness and accuracy of our sample preparation method.

Summarizing the results and arguments of this section, we see that the thermal annealing/structural relaxation process carried out by preparing samples with lower fictive temperatures (i) annihilates free volume present in the glass, leading (ii) to denser packing and thus (iii) to a higher density with density variations of ≈ 0.38% being observed. While points (i) and (ii) represent trends that were expected, point (iii) *quantifies* the degree to which this happens, which is found to be remarkably high since the fully annealed samples (at different fictive temperatures) are all amorphous according to XRD measurements. Since denser packing impedes the flow of atoms past each other, the material's ability to relieve external stress through plastic flow is reduced. Therefore, by purposefully modifying the structural state of a specimen to higher or

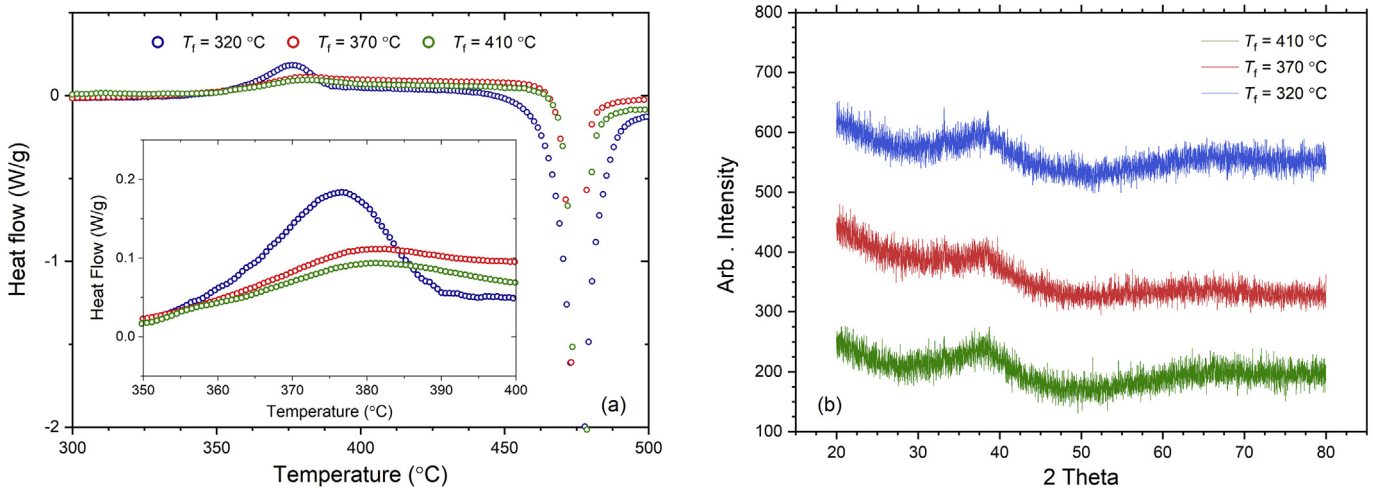

Fig. 2. (a) Differential scanning calorimetry thermograms of $Zr_{44}Ti_{11}Cu_{10}Ni_{10}Be_{25}$ of $T_f = 320\,^\circ$C, $370\,^\circ$C, and $410\,^\circ$C. The inset enlarges the glass transition region where the alloys are able to relax freely, with differences in heat flow directly correlating to the relative differences in the recovered enthalpy. (b) XRD graphs of $Zr_{44}Ti_{11}Cu_{10}Ni_{10}Be_{25}$ BMG samples of $T_f = 320\,^\circ$C, $370\,^\circ$C, and $410\,^\circ$C.

lower densities, we anticipate that its mechanical properties can be adjusted to higher or lower values as needed. The following section will explore *how much* this affects their moduli, hardness, yield strength, and creep response.

3.2. Mechanical properties measurement

3.2.1. Berkovich nanoindentation

Nanoindentation studies indicate a significant difference in the response of the material with a T_f of 320 °C when compared to 410 °C as seen from the average load displacement curves in Fig. 3a. Fig. 3b shows the hardness (measured from the unloading curve) and the effective modulus for the Zr-BMG samples with different T_f. The effective modulus and Oliver-Pharr hardness (unloading hardness) are 126.2 GPa and 6.9 GPa, respectively, for samples with $T_f = 320$ °C, 117.32 GPa and 6.7 GPa for samples with $T_f = 370$ °C, and 110.9 GPa and 6.4 GPa for samples with $T_f = 410$ °C. These values represent a roughly linear increase of the effective modulus and hardness with decreasing T_f, amounting to a relative rise of approximately 14% and 10%, respectively, when the T_f is lowered from its highest value studied here (410 °C) to the lowest value considered (320 °C). Since all three samples are relaxed amorphous alloys with a comparatively low density of casting defects due to the thermoplastic forming process, it is reasonable to correlate the increase in modulus and hardness with the residual amount of free volumes present after annealing (fictive temperature processing). Within this picture, an increase in free volume is thought to affect mechanical properties such as modulus or resistance to plastic deformation in three ways, the first one being a decrease of the resistance to atomic flow through looser packing [69,70], which results in the reduction of geometric constraints. Secondly, we consider that the looser packing leads to increases in the average atomic distances, which weakens atom-atom interactions. Finally, looser packing may generally degrade short-range order, thereby further diminishing the rigidity of a specific local atomic arrangement.

3.2.2. Spherical nanoindentation and creep response

To investigate the creep response of the material as a function of T_f, spherical indentation creep testing has been performed, with Fig. 4a depicting typical load-displacement curves obtained during data acquisition. For creep analysis, this data is then in Fig. 4b plotted as displacement-time curves, with the inset showing creep displacement with time during hold at peak load. Table 1 summarizes the results from the nanoindentation creep experiments. Previous research has shown that the creep behavior of bulk metallic glasses studied using nanoindentation by Berkovich [71–76] and spherical indenters [77] is influenced by the loading rate [78], the composition, and the structure state of the material [71,73]. The creep mechanism in bulk metallic glass (creep flow beneath the indenter) is thought to be due to free volume creation and annihilation, interfacial diffusion, and shear transformation zone evolution [76]. An increase in structural relaxation (i.e., "ageing") has previously been shown to decrease both the rate at which the creep occurs as well as the maximum deformation that is ultimately reached [71].

Due to the more advanced structural relaxation and the related increase in ordering as the T_f is decreased, the deformation during creep and the steady state creep rate $\dot{\varepsilon}_{creep} = \partial h/\partial t$ during hold at 100 mN peak load increases progressively with an increase in T_f. The results agree with the prediction that an increase in ordering would result in a progressive reduction of defects where localized elastic deformations can occur. The reduced modulus E^*, obtained using Hertzian equations for spherical indentation in the elastic region, increases with decreasing fictive temperature, thereby showing a similar trend to the Berkovich nanoindentation results.

3.2.3. Yield strength comparison between different T_f

With respect to quantifying the dependence of density to yield strength, we note that previous research by Yang et al. [79] and by Liu et al. [80] has already shown that higher-density alloys are presumed to have higher yield and fracture strengths when compared to lower-density counterparts. Yang et al. [79] describe this behavior with a *universal scaling law*

$$\tau_y = \frac{3R(T_g - T_r)\rho_r}{M} \cong \frac{\sigma_y}{2} \cong \frac{\sigma_f}{2.2} \tag{6}$$

where τ_y, the maximum shear stress in a BMG upon yielding at room temperature T_r, only depends on the material's T_g, its molar mass M, and its density at room temperature ρ_r. In addition, σ_y is the yield strength under monotonic loading conditions, σ_f is fracture strength of the glass, and R reflects the universal gas constant. Rationalizing the individual terms, the ratio ρ_r/M can be regarded as a measure for the available free volume at T_r while $R(T_g - T_r)$, which is proportional to the energy input needed to enable viscous flow,

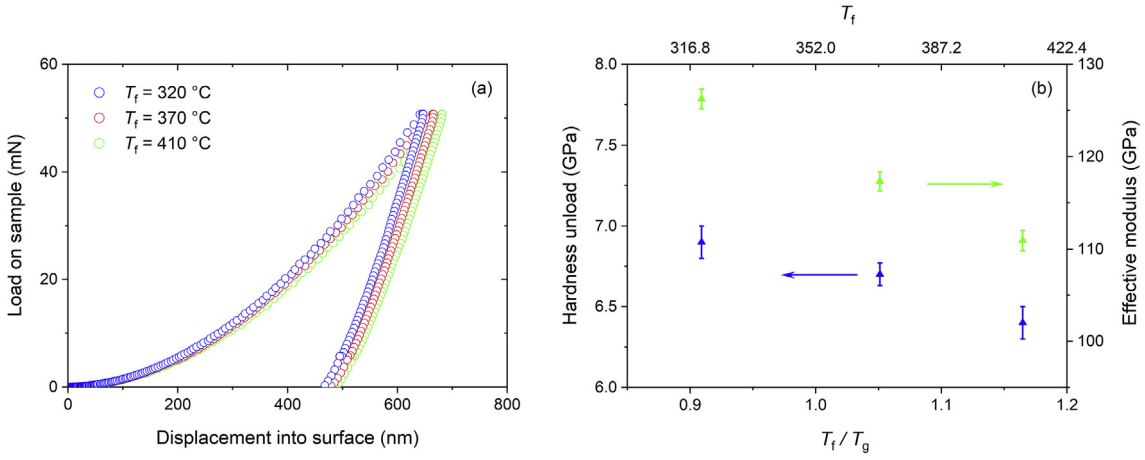

Fig. 3. Results of nanoindentation testing of Zr-BMG processed to reflect three different T_f, namely 320 °C, 370 °C, and 410 °C. (a) Representative curves carried out with 50 mN peak load; (b) average hardness (Oliver-Pharr) obtained from the unloading curves (blue) and average effective modulus (green), both plotted as a function of T_f. (For interpretation of the references to colour in this figure legend, the reader is referred to the Web version of this article.)

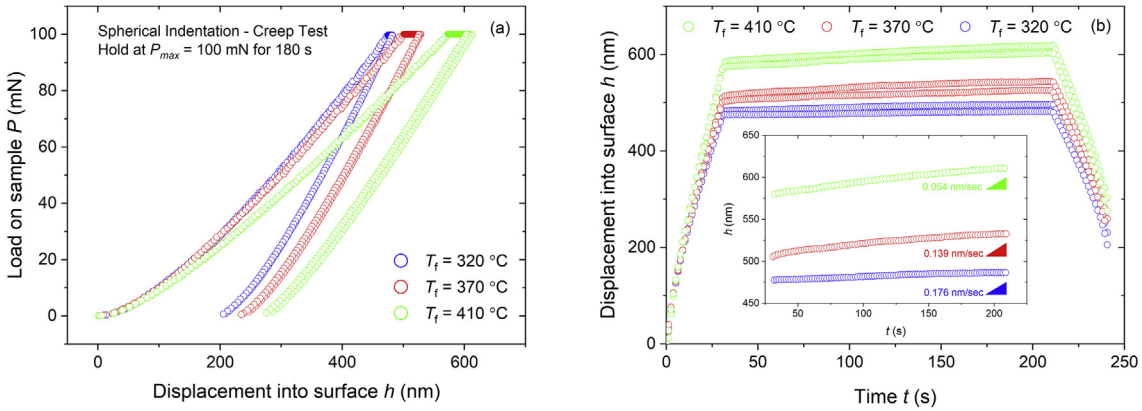

Fig. 4. Creep testing of $Zr_{44}Ti_{11}Cu_{10}Ni_{10}Be_{25}$ processed at three different T_f's of 320 °C, 370 °C and 410 °C using a spherical indenter. (a) Representative load–displacement curves with a peak load of 100 mN and a 180 s hold at maximum load. (b) Quantification of creep using displacement h – time t curves extracted from the data during the hold section of the tests displayed in (a). The inset shows a magnification of the part of the displacement vs. hold time curves at peak load with the steady-state creep rates listed.

Table 1
Creep testing results on Zr-BMG with different fictive temperatures.

Zr-BMG T_f	320 °C	370 °C	410 °C
$\dot{\varepsilon}_{creep}$	0.0545 ± 1.04E-4	0.1394 ± 2.66E-4	0.176 ± 3.03E-4
C_{IT}	2.33 ± 0.87	6.00 ± 0.68	6.41 ± 0.65
h_p (nm)	216.05 ± 12.04	248.24 ± 13.60	282.86 ± 8.95
E^* (Hertz) GPa	110.61 ± 0.25	103.83 ± 0.35	92.49 ± 0.37

highlights the thermodynamic origin of shear band formation, fracture, and yielding in bulk metallic glasses. Since Eq. (6) was found to be valid, e.g., by Fornell et al. [81] for $Zr_{25}Ti_{40}Cu_9Ni_8Be_{18}$ comparing both experimental and theoretical values and by Tan et al. [82] for $Zr_{56}Co_{28}Al_{16}$, it can be used to calculate both τ_y and σ_y. Doing so, we find that τ_y (σ_y) varies from 0.833 GPa (1.667 GPa) for a sample with $T_f = 320$ °C (leftmost data point) to 0.830 GPa (1.660 GPa) for a sample with $T_f = 410$ °C (rightmost data point, please recall that $T_g = 352$ °C. In comparison, the yield strength for the original raw material from Materion corporation was, using different methods, found to be within a 1.8–2 GPa range [20,34,83], which shows similar trends with the results obtained using the universal scaling law.

To compare these expectations with measured values, we plotted in Fig. 5 the yield strength obtained for Zr-BMG samples with different T_f by inserting the density measurements from Sect. 3.2 into the universal scaling law Eq. (6) (blue dots) [79] and then added the equivalent values calculated from Tabor's equation $H/\sigma_y \approx 3$ using the hardness derived from the Berkovich nanoindentation measurements (green dots) [54].

Although the values obtained by Tabor's equation based on hardness measurements are higher, the difference can be attributed to the pile-up corrections which need to be taken into consideration, with yield strength values from hardness measurements for $T_f = 410$ °C being close to the range of yield strengths of 1.8–2 GPa measured by previous researchers [34,83]. Most notably, however, both data sets exhibit a clear, statistically relevant trend with the yield strength decreasing with increasing fictive temperatures, even though this decrease is less prominent for data derived from the density measurements compared to the data obtained from nanoindentation.

3.2.4. Dynamic mechanical analysis

To complement our mechanical properties vs. fictive temperature studies, isochronal DMA was carried out on Zr-BMG samples with different T_f. The variation of the storage modulus G', the loss

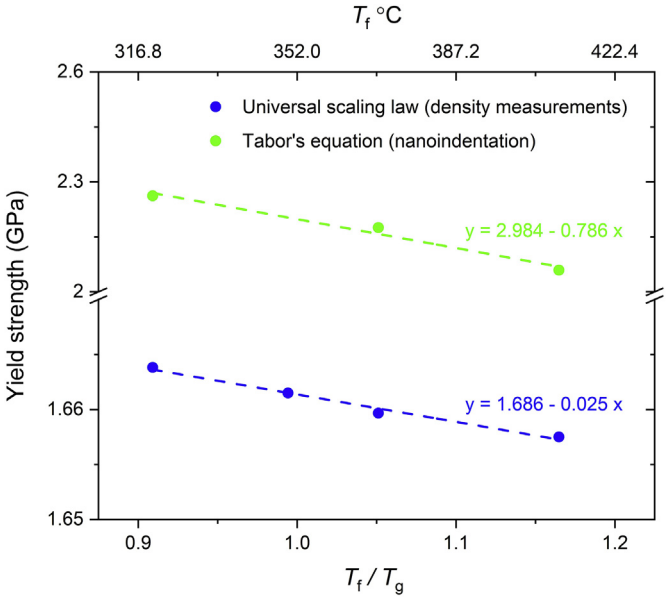

Fig. 5. Yield strength for $Zr_{44}Ti_{11}Cu_{10}Ni_{10}Be_{25}$ of different fictive temperature T_f. Despite different slopes, both the data obtained from density measurements using the universal scaling law Eq. (6) and Tabor's equation ($H/\sigma_y \approx 3$) reveal the clear trend that yield strengths are decreasing for higher T_f's (note that the vertical scale is different for the top and bottom halves of the graph).

modulus G'', and the loss factor $\tan\delta$ in torsion with increasing temperature for Zr-BMGs featuring different fictive temperatures is plotted in Fig. 6. Thereby, we find that G' increases with a decrease in T_f; at room temperature T_r, the measured storage moduli G' of samples with $T_f = 320$ °C, 370 °C, and 410 °C are approximately 20.5 GPa, 18.6 GPa, and 16.5 GPa, respectively, which means that the G' at room temperature of a sample with $T_f = 410$ °C is approximately 24% greater than that of a sample with $T_f = 410$ °C. Fig. 6a displays the storage and loss modulus normalized with regard to their respective storage modulus G_u at room temperature plotted against temperature. As indicated in the figure, three different regions are evident: In the low-temperature region (I), the material is in an amorphous state and the response is, at least on the time scale of the experiment, mostly elastic. As a consequence, the loss modulus almost vanishes (i.e., $G'' \approx 0$), leading to $G_u = G'(T = 25\,°C) \approx G(T = 25\,°C)$. The transition from region (I) to

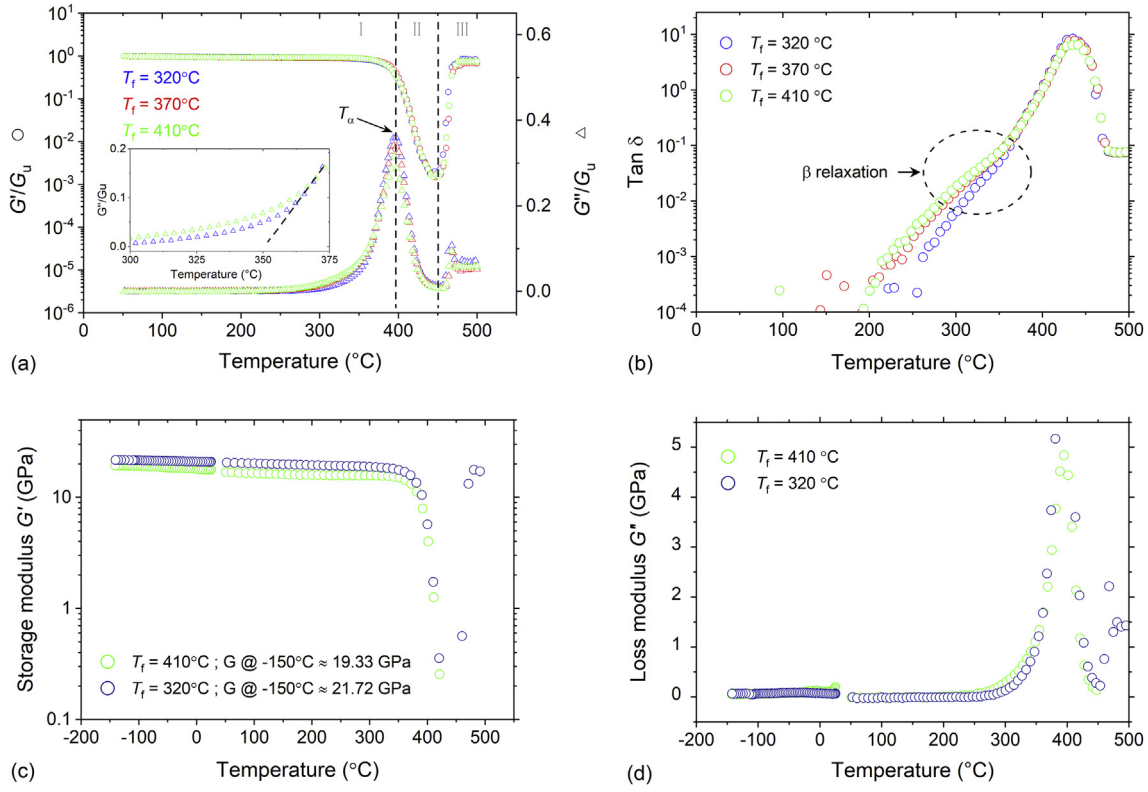

Fig. 6. Dynamic mechanical analysis of $Zr_{44}Ti_{11}Cu_{10}Ni_{10}Be_{25}$ BMG with different T_f's. (a) Normalized storage and loss moduli; (b) tan δ measured in torsion as a function of increasing temperature from 50 °C to 500 °C; (c) storage modulus in torsion from −150 °C to 500 °C for two samples with fictive temperatures of 410 °C and 320 °C, respectively; and (d) loss modulus data complementary to (c).

region (II) is defined by a maximum in G'', located at a temperature T_α; the related peak can be tied to the frequent occurrence of structural relaxations within the glass referred to as α relaxations [76,84,85]. In the mid-temperature region (II), substantial viscosity causes G' to decrease with temperature, until G' and G'' increase again in region (III) due to the progressing degree of crystallization. For comparison, we then plot in Fig. 6b the variation of the loss factor $\tan\delta = G''/G'$ with temperature, which increases for increasing temperatures until it reaches a peak near $T \approx 435$ °C. Fig. 6c is then used to highlight the behavior of G' as a function of temperature. For data points acquired while heating two samples with T_f of 320 °C and 410 °C from T_r up to T_g, a constant decrease in G' is observed, which is expected due to the material's thermal expansion [86].

Subsequent testing of the same samples upon cooling from T_r to −150 °C confirms a matching steady increase of G' with decreasing temperature with no ductile-to-brittle transitions observable within the tested temperature range. Finally, complementary data for the loss modulus (Fig. 6d) reveals that G'' is almost zero at temperatures below T_r, as expected from our earlier discussion.

To continue the discussion, let us note that a secondary β-relaxation peak is often observed in metallic glasses below T_g, which is not found in any of the Zr-BMG samples investigated here. However, it has previously been reported for BMGs containing significant amounts of copper that the β-relaxation peak is influenced by composition, which causes the onset of β relaxation to be at a higher temperature, thereby overlapping with the α-relaxation peak and ultimately resulting in a shoulder or 'excess wing' [85,87,88]. This is most easily seen from Fig. 6b, where the rate at which tan δ increases with temperature accelerates for temperatures higher than $T \approx T_g$. Another reason may be that the enthalpy of mixing for the various atomic pairs in the Zr-BMG is either close to zero or negative, with large fluctuations [89], which may suppress β-relaxation peaks, as suggested by Yu et al. [90]. Finally, we also recover from Fig. 6b that the sample with a T_f of 320 °C has a smaller β-relaxation intensity than samples of T_f of 370 °C and 410 °C. Structural heterogeneities have been found to influence β-relaxation in bulk metallic glass [91,92]; therefore, a glass with higher ordering (T_f of 320 °C) will have to overcome a higher potential energy barrier when initiating flow by activating a previously unsheared shear transformation zone based on the co-operative shear model [93] compared to glasses with either $T_f = 370$ °C or $T_f = 410$ °C, which will result in reduced β-relaxations.

4. Conclusion

In conclusion, we have created glasses with different fictive temperatures by manipulating processing conditions through rapid quenching and annealing. All samples were identified as being amorphous through XRD and DSC; DSC also revealed different degrees of structural relaxation, which was concluded from the fact that the enthalpy recovered during heating increases as fictive temperature decreases. In addition, density measurement exhibit that the density increases as the fictive temperature decreases, which was explained through an increase in ordering and reduction of free volumes. As a result, samples with purposefully set fictive temperatures are found to represent well-defined, structural states that are ideally suited for systematically examining structure-property relationships.

Subsequent mechanical properties testing using

nanoindentation and dynamic mechanical analysis then exposes that the hardness and modulus increase when T_f decreases. With a 14% increase in the effective modulus and a 10% increase in the hardness when T_f changes from 410 °C to 320 °C, this increase is found to be significant. Similarly, the storage modulus in torsion also features an increase from ≈16 GPa to ≈20 GPa when the T_f is lowered from 410 °C to 320 °C. An increase in ordering decreases the intensity of the β-relaxation wing during isochronal DMA. Nanoindentation creep curves disclose differences in the intrinsic deformation mechanisms in samples with different T_f due to changes in the structural state (free volumes and ordering). However, further testing is needed to address the effect of anelastic (recoverable) and viscoplastic (permanent) deformations. Finally, estimating the yield strength from either the universal scaling law using highly precise density measurements or from Tabor's law using hardness values obtained from nanoindentation show similar trends, with both quantitative estimates being close to the yield strength measured by previous researchers.

Author contributions

U.D.S. and A.D conceived and directed the work. A.D designed the experimental procedure. Experiments were conducted by A.D with support by J.K. A.D. analysed the data. A.D, J.K, J.S collaborated with U.D.S. to compose the manuscript. All authors discussed and commented on the manuscript.

Declaration of competing interest

The authors declare that they have no known competing financial interests or personal relationships that could have appeared to influence the work reported in this paper.

Acknowledgements

Financial support by the United States Department of Energy (Grant No. DE-SC0016179) is gratefully acknowledged. Work carried out after 6/1/2019 was supported by the United States National Science Foundation (Grant No. NSF CMMI-1901959). In addition, we thank G. M. Pharr for access to the nanoindenter and S. Suib for access to the facilities at the Institute of Materials Science at the University of Connecticut.

Appendix A. Supplementary data

Supplementary data to this article can be found online at https://doi.org/10.1016/j.jallcom.2019.152979.

References

[1] W. Klement, R.H. Willens, P. Duwez, Non-crystalline structure in solidified gold-silicon alloys, Nature 187 (1960) 869–870.
[2] J. Schroers, W.L. Johnson, Ductile bulk metallic glass, Phys. Rev. Lett. 93 (2004) 255506.
[3] A.L. Greer, E. Ma, Bulk metallic glasses: at the cutting edge of metals research, MRS Bull. 32 (2007) 611–615.
[4] M. Miller, P. Liaw, Bulk Metallic Glasses, Springer, 2008. New York.
[5] C. Suryanarayana, A. Inoue, Bulk Metallic Glasses, CRC Press, 2011.
[6] A. Inoue, Stabilization of metallic supercooled liquid and bulk amorphous alloys, Acta Mater. 48 (2000) 279–306.
[7] A. Peker, W.L. Johnson, A highly processable metallic glass: Zr41.2Ti13.8-Cu12.5Ni10.0Be22.5, Appl. Phys. Lett. 63 (1993) 2342–2344.
[8] G. Kumar, P. Neibecker, Y.H. Liu, J. Schroers, Critical fictive temperature for plasticity in metallic glasses, Nat. Commun. 4 (2013).
[9] W.L. Johnson, Bulk glass-forming metallic alloys: Science and technology, MRS Bull. 24 (1999) 42–56.
[10] C.A. Angell, Formation of glasses from liquids and biopolymers, Science 267 (1995) 1924–1935.
[11] Y.H. Liu, D. Wang, K. Nakajima, W. Zhang, A. Hirata, T. Nishi, A. Inoue, M.W. Chen, Characterization of nanoscale mechanical heterogeneity in a metallic glass by dynamic force microscopy, Phys. Rev. Lett. 106 (2011) 125504.
[12] Y.Q. Cheng, E. Ma, Atomic-level structure and structure-property relationship in metallic glasses, Prog. Mater. Sci. 56 (2011) 379–473.
[13] C. Schuh, T. Hufnagel, U. Ramamurty, Mechanical behavior of amorphous alloys, Acta Mater. 55 (2007) 4067–4109.
[14] T.C. Hufnagel, C.A. Schuh, M.L. Falk, Deformation of metallic glasses: recent developments in theory, simulations, and experiments, Acta Mater. 109 (2016) 375–393.
[15] J. Ketkaew, W. Chen, H. Wang, A. Datye, M. Fan, G. Pereira, U.D. Schwarz, Z. Liu, R. Yamada, W. Dmowski, M.D. Shattuck, C.S. O'Hern, T. Egami, E. Bouchbinder, J. Schroers, Mechanical glass transition revealed by the fracture toughness of metallic glasses, Nat. Commun. 9 (2018) 3271.
[16] A.Q. Tool, Relation between inelastic deformability and thermal expansion of glass in its annealing range, J. Am. Ceram. Soc. 29 (1946) 240–253.
[17] A.Q. Tool, C.G. Eichlin, Variations caused in the heating curves of glass by heat treatment, J. Am. Ceram. Soc. 14 (1931) 276–308.
[18] Y. Waseda, T. Egami, Effect of low-temperature annealing and deformation on the structure of metallic glasses by X-ray-diffraction, J. Mater. Sci. 14 (1979) 1249–1253.
[19] F. Zhang, X.C. Wang, P. Deng, X.M. Qin, J. Tan, The evolution of structural and elastic properties of a Zr-based metallic glass upon annealing below glass transition temperature, Int. J. Mod. Phys. B 33 (2019).
[20] M. Stoica, N. Van Steenberge, J. Bednarcik, N. Mattern, H. Franz, J. Eckert, Changes in short-range order of Zr55Cu30Al10Ni5 and Zr55Cu20Al10Ni10Ti5 BMGs upon annealing, J. Alloy. Comp. 506 (2010) 85–87.
[21] B.B. Medeiros, M.M. Medeiros, J. Fornell, J. Sort, M.D. Baro, A.M. Jorge, Nanoindentation response of Cu-Ti based metallic glasses: comparison between as-cast, relaxed and devitrified states, J. Non-Cryst. Solids 425 (2015) 103–109.
[22] J.C. Qiao, J.M. Pelletier, C. Esnouf, Y. Liu, H. Kato, Impact of the structural state on the mechanical properties in a Zr-Co-Al bulk metallic glass, J. Alloy. Comp. 607 (2014) 139–149.
[23] M. Zhou, K. Hagos, H.Z. Huang, M. Yang, L.Q. Ma, Improved mechanical properties and pitting corrosion resistance of Zr65Cu17.5Fe10Al7.5 bulk metallic glass by isothermal annealing, J. Non-Cryst. Solids 452 (2016) 50–56.
[24] V. Venkatesh, Gouthama, K. Mondal, Effect of cast temperature, size and annealing condition on the serrated flow during nano-indentation of Zr-based bulk metallic glasses, J. Alloy. Comp. 692 (2017) 745–757.
[25] W.J. Wright, T.C. Hufnagel, W.D. Nix, Free volume coalescence and void formation in shear bands in metallic glass, J. Appl. Phys. 93 (2003) 1432–1437.
[26] W. Zhao, J.L. Cheng, H. Cheng, G. Li, Effect of low-temperature annealing on the structure and mechanical properties of Zr-Cu metallic glasses, Mater. Sci. Eng. A Struct. 673 (2016) 239–242.
[27] B. Sarac, A. Bernasconi, J. Wright, M. Stoica, F. Spieckermann, M. Muhlbacher, J. Keckes, X. Bian, G. Wang, J. Eckert, Structural modifications in sub-Tg annealed CuZr-based metallic glass (vol 707, pg 245, 2017), Mater. Sci. Eng. A Struct. 712 (2018), 819–819.
[28] Y.Q. Wang, J.J. Zhang, K. Wu, G. Liu, D. Kiener, J. Sun, Nanoindentation creep behavior of Cu-Zr metallic glass films, Mater. Res. Lett. 6 (2018) 22–28.
[29] P. Murali, U. Ramamurty, Embrittlement of a bulk metallic glass due to sub-T-g annealing, Acta Mater. 53 (2005) 1467–1478.
[30] A. Foroughi, H. Ashuri, R. Tavakoli, M. Stoica, D. Sopu, J. Eckert, Structural modification through pressurized sub-T-g annealing of metallic glasses, J. Appl. Phys. 122 (2017).
[31] C. Minnert, M. Kuhnt, S. Bruns, A. Marshal, K.G. Pradeep, M. Marsilius, E. Bruder, K. Durst, Study on the embrittlement of flash annealed Fe85.2B9.5P4Cu0.8Si0.5 metallic glass ribbons, Mater. Des. 156 (2018) 252–261.
[32] P.N. Zhang, J.F. Li, Y. Hu, Y.H. Zhou, Microstructural evolution during annealing and rolling Zr52.5Cu17.9Ni14.6Al10Ti5 bulk metallic glass, Mater. Sci. Eng. A Struct. 499 (2009) 374–378.
[33] C.T. Moynihan, A.J. Easteal, M.A. Debolt, J. Tucker, Dependence of fictive temperature of glass on cooling rate, J. Am. Ceram. Soc. 59 (1976) 12–16.
[34] D.C. Hofmann, R. Polit-Casillas, S.N. Roberts, J.P. Borgonia, R.P. Dillon, E. Hilgemann, J. Kolodziejska, L. Montemayor, J.O. Suh, A. Hoff, K. Carpenter, A. Parness, W.L. Johnson, A. Kennett, B. Wilcox, Castable bulk metallic glass strain wave gears: towards decreasing the cost of high-performance robotics, Sci. Rep.-Uk 6 (2016).
[35] H. Vogel, The temperature dependence law of the viscosity of fluids, Phys. Z. 22 (1921) 645–646.
[36] G.S. Fulcher, Analysis of recent measurements of the viscosity of glasses. II, J. Am. Ceram. Soc. 8 (1925) 789–794.
[37] T. Waniuk, J. Schroers, W.L. Johnson, Timescales of crystallization and viscous flow of the bulk glass-forming Zr-Ti-Ni-Cu-Be alloys, Phys. Rev. B 67 (2003).
[38] M.E. Launey, R. Busch, J.J. Kruzic, Effects of free volume changes and residual stresses on the fatigue and fracture behavior of a Zr-Ti-Ni-Cu-Be bulk metallic glass, Acta Mater. 56 (2008) 500–510.
[39] L. Shadowspeaker, R. Busch, On the fragility of Nb-Ni-based and Zr-based bulk metallic glasses, Appl. Phys. Lett. 85 (2004) 2508–2510.
[40] J. Lendvai, J. Gubicza, J.L. Labar, Z. Kuli, Effect of crystallization on the deformation behavior of a Zr-based bulk metallic glass, Int. J. Mater. Res. 100 (2009) 439–442.
[41] J. Schroers, The superplastic forming of bulk metallic glasses, JOM-Us 57 (2005) 35–39.

[42] J. Schroers, Processing of bulk metallic glass, Adv. Mater. 22 (2010) 1566–1597.
[43] J. Schroers, N. Paton, Amorphous metal alloys form like plastics, Adv. Mater. Process. 164 (2006) 61–63.
[44] W.C. Oliver, G.M. Pharr, Measurement of hardness and elastic modulus by instrumented indentation: advances in understanding and refinements to methodology, J. Mater. Res. 19 (2004) 3–20.
[45] W.C. Oliver, New nanoindentation and scanning probe tools and techniques, surfaces and interfaces in nanostructured materials and trends in liga, miniaturization, and nanoscale materials, DOI (2004), 299–299.
[46] W.C. Oliver, G.M. Pharr, An improved technique for determining hardness and elastic-modulus using load and displacement sensing indentation experiments, J. Mater. Res. 7 (1992) 1564–1583.
[47] A.P. Ternovskii, V.P. Alekhin, M.K. Shorshorov, M.M. Khrushchov, V.N. Skvortsov, Micromechanical testing of materials by depression, Zavod. Lab. 39 (10) (1974) 1242–1247.
[48] S.I. Bulychev, V.P. Alekhin, M.K. Shorshorov, A.P. Ternovskii, G.D. Shnyrev, Determination of youngs modulus according to indentation diagram, Zavod. Lab. 41 (1975) 1137–1140.
[49] S.I. Bulychev, V.P. Alekhin, Method of kinetic hardness and microhardness in testing impression by an indentor, Ind. Lab. 53 (1987) 1091–1096.
[50] V.P. Alekhin, S.I. Bulychev, Determination of activation volume According to hardness change, Dokl. Akad. Nauk SSSR 238 (1978) 1328–1331.
[51] J.J. Vlassak, W.D. Nix, Measuring the elastic properties of anisotropic materials by means of indentation experiments, J. Mech. Phys. Solids 42 (1994) 1223–1245.
[52] J.J. Vlassak, W.D. Nix, Indentation modulus of elastically anisotropic half-spaces, Philos. Mag. A 67 (1993) 1045–1056.
[53] A. Datye, L. Li, W. Zhang, Y.J. Wei, Y.F. Gao, G.M. Pharr, Extraction of anisotropic mechanical properties from nanoindentation of SiC-6H single crystals, J. Appl. Mech.-T Asme 83 (2016).
[54] D. Tabor, The physical meaning of indentation and scratch hardness,, Br. J. Appl. Phys. 7 (1956) 159.
[55] H.D. Merchant, G.S. Murty, S.N. Bahadur, L.T. Dwivedi, Y. Mehrotra, Hardness-temperature relationships in metals, J. Mater. Sci. 8 (1973) 437–442.
[56] J.R. Cahoon, W.H. Broughton, A.R. Kutzak, The determination of yield strength from hardness measurements, Metall. Trans. 2 (1971) 1979–1983.
[57] H.S. Chen, J.T. Krause, E. Coleman, Elastic constants, hardness and their implications to flow properties of metallic glasses, J. Non-Cryst. Solids 18 (1975) 157–171.
[58] T.B. Matias, V. Roche, R.P. Nogueira, G.H. Asato, C.S. Kiminami, C. Bolfarini, W.J. Botta, A.M. Jorge, Mg-Zn-Ca amorphous alloys for application as temporary implant: effect of Zn content on the mechanical and corrosion properties, Mater. Des. 110 (2016) 188–195.
[59] R.F. Cook, M.L. Oyen, Nanoindentation behavior and mechanical properties measurement of polymeric materials, Int. J. Mater. Res. 98 (2007) 370–378.
[60] F. Mainardi, G. Spada, Creep, relaxation and viscosity properties for basic fractional models in rheology, Eur. Phys. J. Spec. Top. 193 (2011) 133–160.
[61] A.H.W. Ngan, B. Tang, Viscoelastic effects during unloading in depth-sensing indentation, J. Mater. Res. 17 (2002) 2604–2610.
[62] A.S. Argon, Plastic-deformation in metallic glasses, Acta Metall. Mater. 27 (1979) 47–58.
[63] D. Turnbull, M.H. Cohen, On free-volume model of liquid-glass transition, J. Chem. Phys. 52 (1970), 3038-&.
[64] F. Spaepen, Microscopic mechanism for steady-state inhomogeneous flow in metallic glasses, Acta Metall. Mater. 25 (1977) 407–415.
[65] T.W. Wu, F. Spaepen, The relation between embrittlement and structural relaxation of an amorphous metal,, Philos. Mag. B 61 (1990) 739–750.
[66] Z. Evenson, R. Busch, Equilibrium viscosity, enthalpy recovery and free volume relaxation in a Zr44Ti11Ni10Cu10Be25 bulk metallic glass, Acta Mater. 59 (2011) 4404–4415.
[67] A. Slipenyuk, J. Eckert, Correlation between enthalpy change and free volume reduction during structural relaxation of Zr55Cu30Al10Ni5 metallic glass, Scr. Mater. 50 (2004) 39–44.
[68] O. Haruyama, Y. Nakayama, R. Wada, H. Tokunaga, J. Okada, T. Ishikawa, Y. Yokoyama, Volume and enthalpy relaxation in Zr55Cu30Ni5Al10 bulk metallic glass, Acta Mater. 58 (2010) 1829–1836.
[69] W.H. Jiang, F.X. Liu, H. Choo, P.K. Liaw, Effect of structural relaxation on mechanical behavior of a Zr-based bulk-metallic glass, Mater. Trans. 48 (2007) 1781–1784.
[70] W.H. Jiang, F.E. Pinkerton, M. Atzmon, Mechanical behavior of shear bands and the effect of their relaxation in a rolled amorphous Al-based alloy, Acta Mater. 53 (2005) 3469–3477.
[71] A. Castellero, B. Moser, D.I. Uhlenhaut, F.H. Dalla Torre, J.F. Loffler, Room-temperature creep and structural relaxation of Mg-Cu-Y metallic glasses, Acta Mater. 56 (2008) 3777–3785.
[72] W.H. Li, K. Shin, C.G. Lee, B.C. Wei, T.H. Zhang, Y.Z. He, The characterization of creep and time-dependent properties of bulk metallic glasses using nano-indentation, Mater. Sci. Eng. A Struct. 478 (2008) 371–375.
[73] Y.J. Huang, J. Shen, Y.L. Chiu, J.J.J. Chen, J.F. Sun, Indentation creep of an Fe-based bulk metallic glass, Intermetallics 17 (2009) 190–194.
[74] F. Wang, J.M. Li, P. Huang, W.L. Wang, T.J. Lu, K.W. Xu, Nanoscale creep deformation in Zr-based metallic glass, Intermetallics 38 (2013) 156–160.
[75] C. Qiu, P. Zhu, F. Fang, D. Yuan, X. Shen, Study of nanoindentation behavior of amorphous alloy using molecular dynamics, Appl. Surf. Sci. 305 (2014) 101–110.
[76] C. Zhang, J.C. Qiao, J.M. Pelletier, Y. Yao, Thermal activation in the Zr65Cu18Ni7Al10 metallic glass by creep deformation and stress relaxation, Scr. Mater. 113 (2016) 180–184.
[77] T.H. Zhang, J.H. Ye, Y.H. Feng, Y. Ma, On the spherical nanoindentation creep of metallic glassy thin films at room temperature, Mater. Sci. Eng. A Struct. 685 (2017) 294–299.
[78] A. Concustell, J. Sort, A.L. Greer, M.D. Baro, Anelastic deformation of a Pd40Cu30Ni10P20 bulk metallic glass during nanoindentation, Appl. Phys. Lett. 88 (2006).
[79] B. Yang, C.T. Liu, T.G. Nieh, Unified equation for the strength of bulk metallic glasses, Appl. Phys. Lett. 88 (2006).
[80] Y.H. Liu, C.T. Liu, W.H. Wang, A. Inoue, T. Sakurai, M.W. Chen, Thermodynamic origins of shear band formation and the universal scaling law of metallic glass strength, Phys. Rev. Lett. 103 (2009).
[81] J. Fornell, A. Concustell, S. Surinach, W.H. Li, N. Cuadrado, A. Gebert, M.D. Baro, J. Sort, Yielding and intrinsic plasticity of Ti-Zr-Ni-Cu-Be bulk metallic glass, Int. J. Plast. 25 (2009) 1540–1559.
[82] J. Tan, Y. Zhang, B.A. Sun, M. Stoica, C.J. Li, K.K. Song, U. Kuhn, F.S. Pan, J. Eckert, Correlation between internal states and plasticity in bulk metallic glass, Appl. Phys. Lett. 98 (2011).
[83] H.A. Bruck, A.J. Rosakis, W.L. Johnson, The dynamic compressive behavior of beryllium bearing bulk metallic glasses, J. Mater. Res. 11 (1996) 503–511.
[84] J.C. Qiao, J.M. Pelletier, Dynamic mechanical relaxation in bulk metallic glasses: a review, J. Mater. Sci. Technol. 30 (2014) 523–545.
[85] J.C. Qiao, J.M. Pelletier, R. Casalini, Relaxation of bulk metallic glasses studied by mechanical spectroscopy, J. Phys. Chem. B 117 (2013) 13658–13666.
[86] W.H. Wang, The elastic properties, elastic models and elastic perspectives of metallic glasses,, Prog. Mater. Sci. 57 (2012) 487–656.
[87] Z. Wang, H.B. Yu, P. Wen, H.Y. Bai, W.H. Wang, Pronounced slow beta-relaxation in La-based bulk metallic glasses, J. Phys.-Condens. Mater. 23 (2011).
[88] K.L. Ngai, Z. Wang, X.Q. Gao, H.B. Yu, W.H. Wang, A connection between the structural alpha-relaxation and the beta-relaxation found in bulk metallic glass-formers, J. Chem. Phys. 139 (2013).
[89] A. Takeuchi, A. Inoue, Classification of bulk metallic glasses by atomic size difference, heat of mixing and period of constituent elements and its application to characterization of the main alloying element, Mater. Trans. 46 (2005) 2817–2829.
[90] H.B. Yu, K. Samwer, W.H. Wang, H.Y. Bai, Chemical influence on beta-relaxations and the formation of molecule-like metallic glasses, Nat. Commun. 4 (2013).
[91] H.B. Yu, W.H. Wang, H.Y. Bai, Y. Wu, M.W. Chen, Relating activation of shear transformation zones to beta relaxations in metallic glasses, Phys. Rev. B 81 (2010).
[92] H.B. Yu, X. Shen, Z. Wang, L. Gu, W.H. Wang, H.Y. Bai, Tensile plasticity in metallic glasses with pronounced beta relaxations, Phys. Rev. Lett. 108 (2012).
[93] W.L. Johnson, M.D. Demetriou, J.S. Harmon, M.L. Lind, K. Samwer, Rheology and ultrasonic properties of metallic glass-forming liquids: a potential energy landscape perspective, MRS Bull. 32 (2007) 644–650.